Computational Modeling of the Temperature-Induced Structural Changes of Tethered Poly(*N*-isopropylacrylamide) with Self-Consistent Field Theory

Sergio Mendez,[†] John G. Curro,*[,†,‡] John D. McCoy,[§] and Gabriel P. Lopez[†]

Department of Chemical & Nuclear Engineering, University of New Mexico, Albuquerque, New Mexico 87131, Sandia National Laboratories, Albuquerque, New Mexico 87185, and Department of Materials and Metallurgical Engineering, New Mexico Institute of Mining & Technology, Socorro, New Mexico 87801

Received September 8, 2004; Revised Manuscript Received October 26, 2004

ABSTRACT: We modeled the effects of temperature, degree of polymerization, and surface coverage on the equilibrium structure of tethered poly(*N*-isopropylacrylamide) chains immersed in water. We employed a numerical self-consistent field theory where the experimental phase diagram was used as input to the theory. At low temperatures, the composition profiles are approximately parabolic and extend into the solvent. In contrast, at temperatures above the LCST of the bulk solution, the polymer profiles are collapsed near the surface. The layer thickness and the effective monomer fraction within the layer undergo what appears to be a first-order change at a temperature that depends on surface coverage and chain length. Our results suggest that as a result of the tethering constraint, the phase diagram becomes distorted relative to the bulk polymer solution and exhibits closed loop behavior. As a consequence, we find that the relative magnitude of the layer thickness change at 20 and 40 °C is a nonmonotonic function of surface coverage, with a maximum that shifts to lower surface coverage as the chain length increases in qualitative agreement with experiment.

I. Introduction

It is of technological interest to fabricate modified surfaces that allow for reversible modulation of surface properties. Surfaces modified with poly(*N*-isopropylacrylamide) (PNIPAM)[1] have been used in the past to reversibly switch wettability,[2] adhesion of cells[3] and proteins,[4] and membrane porosity[5] with temperature. Aqueous solutions of PNIPAM exhibit a lower critical solution temperature (LCST) near 30 °C. To help optimize this system for future applications, we investigate how temperature affects the equilibrium structure of the tethered PNIPAM.

There have been several experimental efforts to measure the structure of tethered PNIPAM immersed in water at temperatures above and below the LCST. Neutron reflectivity (NR) techniques have been used to measure the composition profile of tethered polymers with varying solvent quality. For upper critical solution temperature (UCST) systems, generally there is a continuous decrease in polymer film thickness as the temperature is lowered below the Θ point.[6,7] Yim and co-workers[8] used NR to determine changes in the structure of tethered PNIPAM with low surface coverage at 20 and 55 °C. Contrary to what was expected, they observed very small changes for 33 and 220 kDa chains. In a later study, Yim and co-workers[9] reported significant changes in the monomer segment density profiles over a series of temperatures for tethered PNIPAM with much higher surface coverage. These studies suggest that molecular weight and surface coverage might play an important role in the temperature response. Balamurugan and co-workers[10] demonstrated that surface plasmon resonance techniques could be used to probe the index of refraction of tethered PNIPAM near the surface. Atomic force microscopy techniques have also been used to characterize the structure of tethered PNIPAM immersed in water at ∼25 and 40 °C.[11,12]

Various theoretical approaches have been used to understand the equilibrium structure of polymers tethered to a wall.[13−15] Alexander[16] and deGennes[17,18] developed scaling theories for the dependence of layer thickness on surface coverage and molecular weight. Self-consistent field (SCF) theory has been adapted to the tethered polymer case by various investigators.[19−25] In the limiting case of highly stretched, high molecular weight chains, Milner et al.[26−28] and Cosgrove[29] solved the SCF theory equations analytically to obtain segment density profiles that are parabolic. An analytical mean-field theory was reported by Zhulina and co-workers[30] who proposed a free energy functional consisting of free energy of mixing and elastic terms. In this theory, the distribution of chain ends is obtained from minimization of the free energy. A somewhat simpler version was developed by Pincus[31] and used by Halperin[32] who assumed the form of the chain end distribution.

The effect of solvent quality on the structure of tethered polymers has been studied with computer simulations. Grest and co-workers have performed molecular dynamics (MD) simulations for tethered polymers. They modeled these systems with explicit[33] and implicit[34,35] solvent for a range of solvent qualities.[36,37] Lai and Binder used Monte Carlo techniques to study tethered polymers in various solvent qualities.[38] They reported a continuous decrease in the first moment of the segment density profile with decreasing temperature. Under poor solvent conditions, they observed lateral inhomogeneities in the film density.

Baranowski and Whitmore used numerical SCF theory to model experimental neutron reflectivity data of

[†] University of New Mexico.
[‡] Sandia National Laboratories
[§] New Mexico Institute of Mining & Technology.

10.1021/ma048156x CCC: $30.25
Published on Web 12/10/2004

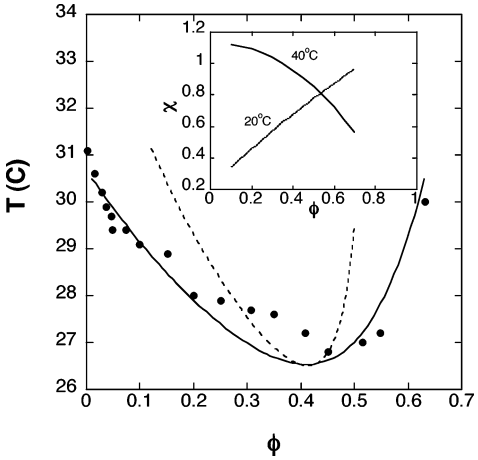

Figure 1. Phase diagram, in the infinite chain limit, predicted from the experimental results of Afroze et al.[46] using a composition and temperature dependent χ parameter with the parameters displayed in Table 1. The solid curve is the bimodal, the dashed curve is the spinodal line, and the points are the data from ref 46. The inset shows the composition dependence of χ at two different temperatures.

tethered polystyrene in two solvent qualities. In their first study,[39] they modeled the experimentally determined[40] structure of tethered polystyrene immersed in a good solvent; subsequently, they modeled[22] experimental NR data[41] of tethered polystyrene in a Θ solvent. They examined the effects of surface coverage and molecular weight on the segment density profiles and found good agreement between theory and experiments.

Karlstrom and co-workers[42] employed a lattice SCF theory for modeling end-grafted poly(ethylene oxide) (PEO) immersed in water. High molecular weight PEO in aqueous solution is known to exhibit an UCST near 100 °C. A two-state model of PEO was proposed in an earlier paper[43] to obtain semiquantitative agreement with the experimental phase diagram of unbound PEO in water. With this two-state model, they predicted only minor changes in the segment density profiles as the temperature was varied from 27 to 327 °C.

Baulin, Halperin, and co-workers[44,45] generalized the mean-field theory of Pincus[31] by introducing a concentration and temperature dependent χ parameter to provide a more a realistic model of tethered polymers in aqueous solution. They reported that a χ with strong concentration dependence leads to the possibility of vertical phase separation within a brush with high surface coverage. They applied their theory to the case of tethered PNIPAM immersed in water[44] by using the concentration and temperature dependent χ parameter reported by Afroze and co-workers[46] for aqueous PNIPAM solutions.

In Figure 1, we have plotted a fit to the phase diagram of the PNIPAM/water solution measured by Afroze and co-workers.[46] The experimental data were fit to Flory–Huggins theory with a χ parameter that depends on composition and temperature as shown in the inset. The inset in Figure 1 displays the composition dependence of χ at 20 and 40° C. Note that at a composition of $\phi = 0.53$ the temperature dependence of χ changes from positive (below) to negative (above). Note also that this is an LCST system where the solution undergoes phase separation at approximately 25−30 °C, the exact value depending on the composition and molecular weight. The purpose of this investigation is to study the difference in the structure of the tethered PNIPAM near the surface above and below the LCST of the bulk solution. Following the idea of Baulin and Halperin[44] in their analytical approach, we use the experimental data of Afroze et al. as input to our numerical SCF theory to deduce composition profiles as a function of molecular weight, surface coverage and temperature.

II. Theory

In this paper we use a SCF theory that is a generalization of the density functional theory (DFT) of McCoy, Ye, and Curro[47,49] for tethered polymers. They applied DFT to tethered, athermal polymers immersed in either an explicit or continuum solvent.[47] For the case of explicit solvent, they obtained close agreement between DFT, MD simulations, and single-chain mean field theory.[48] Applying DFT to tethered polymers in a continuum solvent, they again found close agreement with results from MD simulations.[47] They also applied DFT to tethered polymers in an implicit or continuum solvent to study the effect of temperature on the tethered chain structure. With certain approximations, they adapted DFT to conventional SCF theory and found agreement with results from MD[47] simulations.

In this approach[47] the density profiles $\rho_p(z)$ and $\rho_s(z)$ of polymer and solvent are calculated self-consistently from the coupled functional equations

$$\rho_\alpha(z) = F[U_p^0(z), U_s^0(z)]$$
$$U_\alpha^0(z) = G[\rho_p(z), \rho_s(z)] \quad (1)$$

where z is the distance from the surface and $U_\alpha^0(z)$ is an external field for polymer or solvent (α = p, s) designed to mimic the effects of solvent and other chains on a given tethered chain or solvent molecule. The first of these equations represents the calculation of the density profile of a single tethered chain, or solvent molecule, in the external field. The second part of eq 1 represents the calculation of the external field from $\rho_p(z)$ or $\rho_p(z)$ and represents the essential approximation that distinguishes one DFT theory from another. Here we employ the approach of Chandler, McCoy, and Singer,[50] which involves a functional Taylor series expansion of the free energy. The details are discussed in several applications to polymers[47,51−53] and will only be briefly sketched here. The free energy difference $\Delta W[\rho_p(z), \rho_s(z)]$ between the tethered chain system and an *ideal* system is expanded to quadratic terms about a *reference* system of untethered macromolecules in bulk solution. The ideal system is defined to have the same polymer and solvent profiles as the real system, and is introduced to approximately cancel out cubic and higher order terms in the expansion. Obviously, the closer the ideal system is to the real system the more accurate the expansion will be. For our purposes, we choose the ideal system to consist of noninteracting solvent sites and freely jointed chains tethered to a surface in the presence of the ideal fields $U_p^0(z)$ and $U_s^0(z)$. Minimization of the Grand potential free energy through $\delta\Delta W/\delta\rho_\alpha(z) = 0$ leads to the following expressions for the ideal polymer and solvent fields[51−53]

$$\beta U_p^0(r) = \beta U_p(r) - \sum_{\gamma=s,p} \int C_{p,\gamma}(r - r')\Delta\rho_\gamma(r')\, d\mathbf{r}'$$
$$\beta U_s^0(r) = \beta U_s(r) - \sum_{\gamma=s,p} \int C_{s,\gamma}(r - r')\Delta\rho_\gamma(r')\, d\mathbf{r}' \quad (2)$$

where $\beta = 1/k_BT$ and the $C_{\alpha\gamma}(r)$ are the direct correlation functions[54,55] for the homogeneous polymer solution reference system. $U_p(r)$ and $U_s(r)$ are the fields due to the presence of the wall acting on the polymer and solvent, respectively. The terms $\Delta\rho_\gamma = \rho_\gamma(z) - \rho_{\gamma,\mathrm{ref}}$ are the differences between the polymer or solvent density profiles and their corresponding values in the reference system. Note that the convolution integrals in eq 2 imply that the polymer and solvent fields at position r are nonlocal in the sense that they depend on the direct correlation functions, not just at r but over a range of positions. The direct correlation functions can be found from solving for the structure of the homogeneous polymer solution and contain information about the finite size of the monomer (or solvent) and its effect on the packing in the bulk liquid mixture. Inclusion of nonlocality in the calculation of the density profile is important to capture packing-induced structure near the surface.

In this work our main interest is in the density profiles on longer length scales on the order of the radius of gyration R_g of the tethered macromolecules. Hence we simplify our fields by approximating the direct correlation functions as being short-range according to $C_{\alpha\gamma}(\mathbf{r}) = \hat{C}_{\alpha\gamma}(0)\delta(\mathbf{r})$ where the caret denotes the Fourier transform. Substitution of this approximation into eq 2 leads[47,49] to the following simplified, local fields

$$\beta U_p^0(z) = \beta U_p(z) - [\hat{C}_{pp}(0) - \hat{C}_{ps}(0)][\rho_p(z) - \rho_T] + \lambda(z)$$
$$\beta U_s^0(z) = \beta U_s(z) - [\hat{C}_{sp}(0) - \hat{C}_{ss}(0)][\rho_p(z) - \rho_T] + \lambda(z) \quad (3)$$

where $\rho_T = \rho_p + \rho_s$ is the total density of polymer and solvent and is held fixed. In obtaining eq 3 from eq 2, we have dropped certain constants that are unimportant in the calculation of the density profiles. The $\lambda(z)$ term is a Lagrange multiplier inserted to enforce incompressibility. For a compressible system this undetermined multiplier can be set to zero.

Thus far in our analysis we have not specified the reference system about which the free energy is expanded. For untethered chains and solvent under confinement, the obvious choice of a reference system would be the corresponding bulk solution at a concentration that would exist infinitely far from the surface. In the case of our tethered chains in solution, this would correspond to pure solvent since the grafting constraint confines the chains near the substrate. Since we are free to choose the reference system, we take it instead to consist of a bulk polymer solution at a concentration equal to the average concentration within the polymer brush.

$$\rho_{p,\mathrm{ref}} = \langle\rho_p\rangle = \frac{\int_0^\infty \rho_p^2(z)\,dz}{\int_0^\infty \rho_p(z)\,dz} \quad (4)$$

Thus, our reference system is coupled indirectly to the polymer profile through eq 4. This coupling reintroduces a nonlocal aspect to the field.

As was done by Baulin and Halperin[44] in their analytical theory, our intention in this paper is to use the experimentally determined phase diagram as input to DFT theory in order to predict the density or composition profile of the PNIPAM tethered chains.

Table 1. Parameters in Eq 8 for Describing the Temperature and Composition-Dependent χ Parameter of Aqueous PNIMPAM Solutions Obtained by Afroze and Co-Workers[46]

i	A_i	B_i (K^{-1})
0	−12.947	0.044959
1	17.920	−0.056944
2	14.814	−0.051419

Toward this end we employ the incompressible, mean field Flory−Huggins theory[56] to obtain the direct correlation functions in eq 3. The direct correlation functions in the zero wave vector limit can be written as[49,54,55]

$$\hat{C}_{pp}(0) - \hat{C}_{ps}(0) = \frac{1}{N\rho_p} - \hat{S}_{pp}^{-1}(0) + \hat{S}_{ps}^{-1}(0)$$
$$\hat{C}_{ps}(0) - \hat{C}_{ss}(0) = -\frac{1}{\rho_s} - \hat{S}_{ps}^{-1}(0) + \hat{S}_{ss}^{-1}(0) \quad (5)$$

where N is the number of monomers and the $\hat{S}_{\alpha\gamma}^{-1}(k)$ are the various inverse structure factors. Following Kirkwood and Buff,[57] the inverse structure factors in the zero wave vector limit can be related to the Helmholtz free energy of mixing, A_{mix}.

$$\hat{S}_{\alpha\gamma}^{-1}(0) = \frac{1}{k_BTV}\left(\frac{\partial^2 A_{mix}}{\partial\rho_\alpha\partial\rho_\gamma}\right)_{T,V} \quad (6)$$

Substitution of eq 6 into eq 5 yields

$$\hat{C}_{pp}(0) - \hat{C}_{ps}(0) = \frac{1}{N\rho_p} - \frac{1}{Vk_BT}\left(\frac{\partial^2 A_{mix}}{\partial\rho_p^2}\right)_{TV} + \frac{1}{Vk_BT}\left(\frac{\partial^2 A_{mix}}{\partial\rho_p\partial\rho_s}\right)_{TV}$$
$$\hat{C}_{ps}(0) - \hat{C}_{ss}(0) = -\frac{1}{\rho_s} - \frac{1}{Vk_BT}\left(\frac{\partial^2 A_{mix}}{\partial\rho_p\partial\rho_s}\right)_{TV} + \frac{1}{Vk_BT}\left(\frac{\partial^2 A_{mix}}{\partial\rho_s^2}\right)_{TV} \quad (7)$$

Afroze and co-workers[46] fit their experimental phase diagram of the PNIPAM/water system with a composition and temperature-dependent χ parameter of the form (see Figure 1)

$$\chi(\phi,T) = \sum_{i=0}^{2}(A_i + B_iT)\phi^i = \sum_{i=0}^{2}\chi_i(T)\phi^i \quad (8)$$

The A_i and B_i parameters determined by Afroze et al.[46] are given in Table 1. With these parameters, the temperature dependence of χ can be seen from the inset in Figure 1 to change sign at a volume fraction of 0.53. This causes the spinodal temperature to diverge at this volume fraction. One should exercise caution in applying eq 8 at temperatures and volume fractions much beyond the range of the experimental data used to fit A_i and B_i. For PNIPAM solutions, the Flory−Huggins free energy of mixing can then be written as

$$\beta A_{mix} = V\left[\frac{\rho_p}{N}\ln\phi_p + \rho_s\ln(1-\phi_p) + \rho_s\sum_i\chi_i(T)\phi^{i+1}\right] \quad (9)$$

After taking the appropriate derivatives followed by

substitution into eqs 7 and 3, we obtain the polymer and solvent fields

$$\beta U_{\mathrm{p}}^{0}(z) = \beta U_{\mathrm{p}}(z) + \left[1 - \frac{1}{N} - 2(\chi_0 + 2\chi_1 + 3\chi_2)\langle\phi_{\mathrm{s}}\rangle + 6(\chi_1 + 3\chi_2)\langle\phi_s\rangle^2 - 12\chi_2\langle\phi_{\mathrm{s}}\rangle^3\right][\phi_{\mathrm{p}}(z) - 1] + \lambda(z)$$

$$\beta U_{\mathrm{s}}^{0}(z) = \beta \mathrm{U}_{\mathrm{s}}(z) + \left[1 - \frac{1}{N} - 2(\chi_0 - \chi_1)\langle\phi_{\mathrm{p}}\rangle + 6(\chi_1 - \chi_2)\langle\phi_{\mathrm{p}}\rangle^2 + 12\chi_2\langle\phi_{\mathrm{p}}\rangle^3\right][\phi_{\mathrm{p}}(z) - 1] + \lambda(z) \quad (10)$$

where $\phi_\alpha = \rho_\alpha/\rho_{\mathrm{T}}$ is the volume fraction of polymer or solvent. In eq 10 we have written the reference system volume fraction as $\langle\phi_{\mathrm{p}}\rangle = \langle\rho_{\mathrm{p}}\rangle/\rho_{\mathrm{T}}$ to be evaluated from the density profile from eq 4.

Given the ideal polymer and solvent fields, we now consider the functional F in the first part of eq 1 for the calculation of the polymer and solvent profiles. Our choice of a single-site solvent in the ideal system allows us to solve for the solvent profile $\rho_{\mathrm{s}}(z)$ directly from the ideal solvent field.

$$\rho_{\mathrm{s}}(\mathbf{r}) = \rho_{\mathrm{s,ref}} \exp(-\beta U_{\mathrm{s}}^{0}) \quad (11a)$$

Because of chain connectivity, the form of the *F*-functional for the tethered polymer is much more complex and can be written formally as

$$\rho_{\mathrm{p}}(\mathbf{r}) = \sum_{i=1}^{N}\langle\delta(\mathbf{r}_i - \mathbf{r})\rangle$$

$$\langle\delta(\mathbf{r}_i - \mathbf{r})\rangle = \frac{\int\delta(\mathbf{r}_i - \mathbf{r})\mathrm{Z}(\mathbf{r}_i)\,\mathrm{d}\mathbf{r}_i}{\int Z(\mathbf{r}_i)\,\mathrm{d}\mathbf{r}_i}$$

$$Z(\mathbf{r}_i) = \mathrm{e}^{-\beta \mathrm{U}_{\mathrm{i}}^{0}}\int \ldots \int\delta(\mathbf{r}_1 - \mathbf{r}_0)\tilde{S}(\mathbf{r}_1 \ldots \mathbf{r}_N)\exp(-\sum_{j\neq \mathrm{i}}\beta U_j^0)\prod_{j\neq \mathrm{i}}\mathrm{d}\mathbf{r}_j \quad (11b)$$

where site 1 of the polymer is constrained to be tethered to the surface at $\mathbf{r}_0$. All the chain connectivity constraints and intrachain interactions are contained in $\tilde{S}(\mathbf{r}_1 \ldots \mathbf{r}_N)$. In this work our ideal system is a freely jointed chain of bond length σ for which we can write

$$\tilde{S}(\mathbf{r}_1 \ldots \mathbf{r}_{\mathrm{N}}) = \delta(r_{1,2} - \sigma) \ldots \delta(r_{N-1,N} - \sigma) \quad (12)$$

In this case, eq 11b can be solved numerically using Fourier transforms as discussed in detail in ref 47. Note that with our method of solution, we do not make the Gaussian approximation commonly made in other versions of SCF theory and the chains are of finite extensibility. For more realistic models with excluded volume interactions and chain stiffness, the chain is non-Markovian, and eq 11b can only be solved through a single-chain simulation.

In this work, eqs 10 and 11 are solved self-consistently for the density profiles of tethered PNIPAM macromolecules in aqueous solution. The inputs to our SCF theory are N, σ, ρ_{A}, and χ where the surface coverage ρ_{A} is the number of freely jointed chains per unit area. Here the χ parameter is supplied from the experimental phase diagram for aqueous PNIPAM solutions. Alternatively, one could employ simulation or PRISM theory to provide the required input concerning the structure of the reference system consisting of the homogeneous polymer solution.

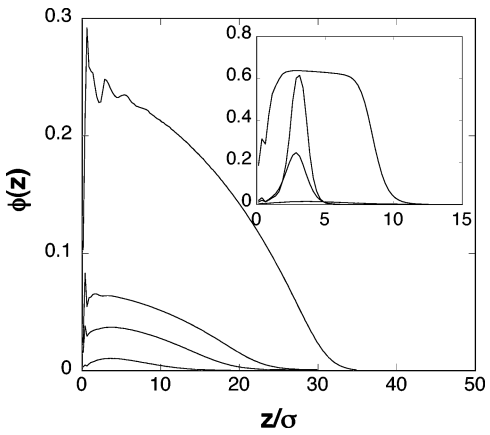

Figure 2. Polymer volume fraction profiles for $N = 100$ and various $\rho_{\mathrm{A}}\sigma^2$ (from low to high, 0.001, 0.005, 0.01, 0.05). The profiles in were calculated at 20 °C (main plot) and 40 °C (inset), respectively. Note that the *y*-axis for both plots are different.

III. Results and Discussion

The SCF equations were solved self-consistently using numerical methods described previously.[47,49] The z-axis was divided into a grid with spacing of 0.25σ and 600 Fourier components were used in the numerical solution of the polymer density profile. The segment density profile, $\rho_{\mathrm{p}}(z)$ is determined through an iterative scheme where an initial profile is used to calculate the external field, $U^{\circ}(z)$, which is then used to calculate a new $\rho_{\mathrm{p}}(z)$. To stabilize these iterations, a mixing coefficient was utilized (=0.10). A convergence criteria requiring that the maximum difference between the $\rho_{\mathrm{p}}(z)$ in consecutive iterations be less than 0.1% was employed. For all SCF theory calculations, the total density, $\rho_{\mathrm{T}}\sigma^3$, was set equal to 1 for convenience.

We first used our theory to determine how the polymer surface coverage ρ_{A} affects the volume fraction profile, $\phi(z)$, while keeping the chain length constant. In Figure 2 we present the profiles for $N = 100$ and $\rho_{\mathrm{A}}\sigma^2 = 0.001$, 0.005, 0.01, and 0.05 at 20 and 40 °C. At low temperatures, we expect water to be a good solvent and the PNIPAM chains to be well solvated; at high temperature, we expect the water to be a poor solvent and the PNIPAM chains to have a more compacted conformation.[9] At 20 °C, the profiles can be seen to be approximately parabolic, and the chains become more stretched with increasing surface coverage. When the profiles are calculated at the higher temperature, the polymer chains are collapsed (see inset) as measured by the maximum extent, arbitrarily defined as the value of z/σ at $\phi = 0.02$, which decreases from 35 at 20 °C to 12 at 40 °C for $\rho_{\mathrm{A}}\sigma^2 = 0.05$. The profiles in the inset of Figure 2 at the higher temperature are characterized by peaks and exclusion zones at the wall. There is a maximum in $\phi(z)$ away from the surface because at 40 °C water is a poor solvent, and the polymer, in an attempt to minimize contact with the water, segregates into "drops". This is qualitatively seen experimentally in refs 6 and 41.

Most of the profiles in this investigation, including those in Figure 2, were calculated with the wall potential $U_{\mathrm{p}}(z)$ in eq 10 being a hard wall, i.e., there were no attractive interactions between the monomers and the

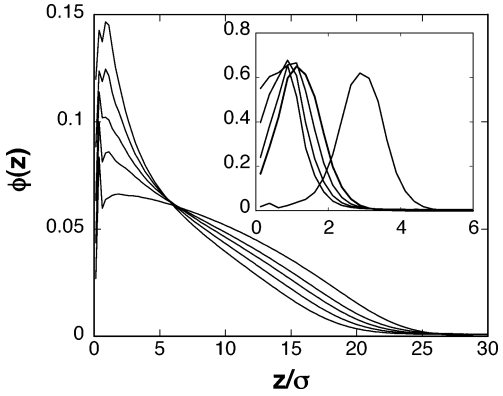

Figure 3. Polymer volume fraction profiles, $\phi(z)$, for $N = 100$ and $\rho_A\sigma^2 = 0.01$ with attractive interactions between monomers and the wall, i.e., $U_p(z) = -c/z$. The strength is varied through c (from low to high $\phi(z)$ near wall 0, 0.2, 0.3, 0.4, 0.5). The profiles were calculated at 20 (main plot) and 40 °C (inset), respectively. Note that the x- and y-axes for both plots are different.

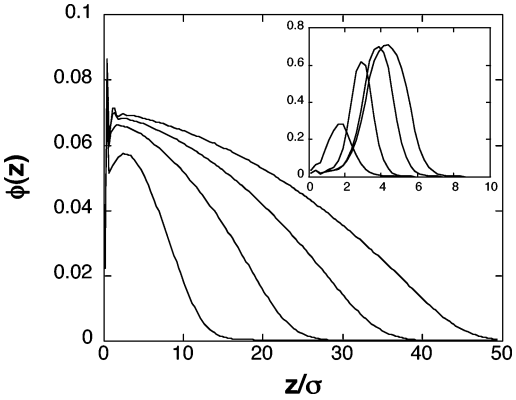

Figure 4. Polymer volume fraction profiles for $\rho_A\sigma^2 = 0.01$ and various N (from left to right, 50, 100, 150, 200). The profiles were calculated at 20 °C (main plot) and 40 °C (inset), respectively. Note that the x- and y-axes for both plots are different.

wall. For real tethered polymers, there might be, for example, van der Waals, electrostatic or dipole interactions. To mimic the attractive interaction between a charge and a nonpolar surface,[58] we performed SCF theory calculations with an attractive tail having the form

$$\beta U_p(z) = \infty, \quad z \le \sigma/2$$
$$\beta U_p(z) = -c/z, \quad z > \sigma/2 \tag{13}$$

where the strength of the interaction can be varied through the constant, c. For chains with $N = 100$ and $\rho_A\sigma^2 = 0.07$ at 20 and 40 °C, we see in Figure 3 that as the attraction strength c increases, the polymer profiles shift toward the wall. At 20 °C, the profiles are no longer parabolic, and the increase in c leads to a sharp rise in the profile very close to the wall. At the higher temperature shown in the inset, the peak is shifted closer to the wall with increasing c, and eventually the tendency to form the drops seen in Figure 2 disappears as polymer accumulates near the wall. Qualitatively similar results were found for quadratic and cubic forms of the wall attraction potential.

The effect of degree of polymerization, N, was explored for tethered polymers with constant surface coverage ($\rho_A\sigma^2 = 0.01$). $\phi(z)$ values for $N = 50$, 100, 150, and 200 at 20 and 40 °C are shown in Figure 4, respectively. As the number of monomers per chain is increased, the polymer at 20 °C extends away from the wall. The features very close to the wall may not be accurately predicted since, in view of the delta function approximation of the direct correlation functions, we do not expect to capture local packing effects. At the higher temperature, the polymer profile is more collapsed as the unfavorable monomer/solvent interactions increase the tendency of polymer segments to be near each other. The centers of the peaks move farther from the wall with increasing chain length.

The overall thickness of the tethered polymer layer can be described by $\langle z \rangle$, twice the first moment of the $\phi(z)$ distribution

$$\langle z \rangle = \frac{2\int z\phi(z)\,dz}{\int \phi(z)\,dz} \tag{14}$$

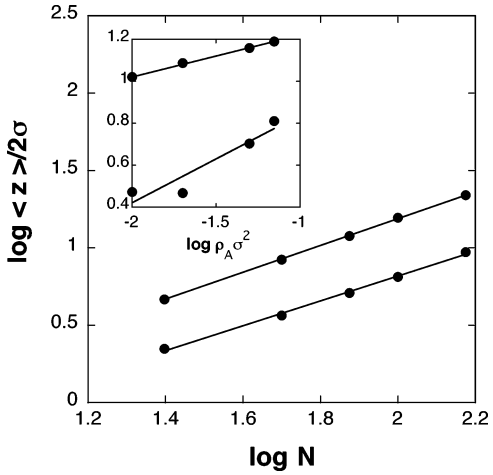

Figure 5. Logarithmic plot of the first moment $0.5\langle z \rangle/\sigma$ of the profile vs chain length (main plot) and surface coverage (inset). The results in both plots are for $T = 20$ °C (upper line) and 40 °C (lower line).

The factor of 2 ensures that eq 14 reduces to the layer thickness for a step density profile. In Figure 5 we have plotted $\langle z \rangle$ as a function of chain length N and surface coverage (inset) at 20 and 40 °C. It can be seen that the average thickness exhibits power law behavior $\langle z \rangle \sim \sigma(\rho_A\sigma^2)^\alpha N^\gamma$. In the strongly overlapped regime where the average spacing between tethered chains is much less than R_g of the polymer in solution (i.e. $(\rho_A\sigma^2)^{-1/2} \ll N^\nu$), scaling arguments[16,17] give $\alpha = (1 - \nu)/2\nu$ and $\gamma = 1$ where ν is the Flory exponent. Hence $\alpha = 1/3$, $1/2$, and 1 for good, Θ, and poor solvents respectively in this regime. From the slopes of the plots in Figure 5 we estimate $\alpha = 0.20$, $\gamma = 0.86$ at 20 °C, and $\alpha = 0.42$, $\gamma = 0.80$ at 40 °C. For the range of surface coverages ($\rho_A\sigma^2 = 0.01$ to 0.1) and chain lengths ($N = 25-150$) studied here, the strongly overlapping conditions are not rigorously satisfied. From neutron reflectivity experiments on tethered PNIPAM chains in the presence of water, Yim and co-workers[59] found that $\gamma = 0.55$ at 20 °C and 0.81 at 41 °C for relatively high surface coverage.

The focus of this investigation is on how temperature affects the equilibrium structure of tethered PNIPAM. The effects of temperature are included in $\chi(\phi,T)$ using the parameters in Table 1. For LCST systems, the solvent quality is expected to decrease with increasing temperature where a phase transition occurs at the demixing (or cloud-point) temperature. At temperatures

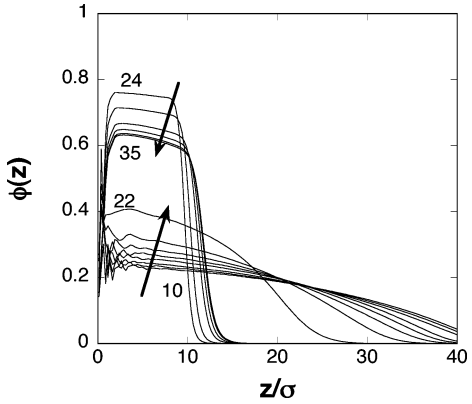

Figure 6. Polymer volume fraction profiles for $N = 100$ and $\rho_A\sigma^2 = 0.07$ over a series of temperatures (10° to 35 °C) are shown. The arrows point in direction of increasing temperature

above the demixing temperature, the solution phase separates into a polymer rich phase and a solvent rich phase. Thus, we expect the dimensions of the tethered PNIPAM chains to decrease with increasing temperature with a sharp transition occurring at an intermediate temperature. Along this line of reasoning, we also expect the transition for the tethered PNIPAM to be a function of surface coverage analogous to the concentration dependence of the demixing temperature of the bulk polymer solution shown in Figure 1.

The SCF theory was used to calculate $\phi(z)$ over a range of temperatures (10−35 °C) for chains with $N = 100$ and $\rho_A\sigma^2 = 0.07$. As presented in Figure 6, $\phi(z)$ at the lowest temperature indicates that the polymer extends into the solvent. From 10 to 22 °C, the chains are seen to contract gradually with decreasing solvent quality. There is a dramatic change in the profile when going from 22 to 24 °C, presumably driven by the LCST of the bulk solution. At temperatures of 24 °C and greater, the profiles are steplike. In the high-temperature regime, the maximum in $\phi(z)$ unexpectedly decreases gradually and the profiles broaden with increasing temperature.

The corresponding first moments of the volume fraction profiles from Figure 6 are presented as a function of temperature in Figure 7a for various chain lengths and Figure 7b for a range of surface coverage. We arbitrarily define the "transition" temperature as the temperature where $\langle z \rangle$ exhibits the greatest magnitude in slope. At low temperatures below the transition, the SCF theory indicates that $\langle z \rangle$ decreases gradually with increasing temperature due to the decreasing solvent quality. Interestingly, in some cases a minimum is observed immediately above the transition and $\langle z \rangle$ increases gradually with increasing temperature. Thus, the temperature dependence of the thickness can be nonmonotonic and of opposite sign below and above the transition. This can be attributed to the concentration dependence of χ, depicted in the inset of Figure 1 based on the parameters of Afroze et al.[46] given in Table 1. As mentioned earlier, χ has opposite temperature dependence at low and high concentration. At low ϕ, χ at 40 °C is greater than χ at 20 °C, i.e., the solvent becomes poorer with increasing temperature. However, at high ϕ (>0.53), the reverse is true: the solvent becomes better with increasing temperature. Below the transition the chains extend into the solvent and the average concentration $\langle \phi \rangle$ within a brush is small. Hence χ increases and $\langle z \rangle$ decreases with temperature. Conversely, above the transition the chains are more compact and the average concentration within a layer increases. Although a detailed comparison was not performed, the predictions shown in Figures 7 are in qualitative agreement with experimentally determined thicknesses $\langle z \rangle$ of tethered PNIPAM performed by Yim, and co-workers.[9] In both experiments and theory, the change in $\langle z \rangle$ occurs over a broad temperature range, with gradual changes at low temperature, and at high temperatures $\langle z \rangle$ remains practically independent of temperature.

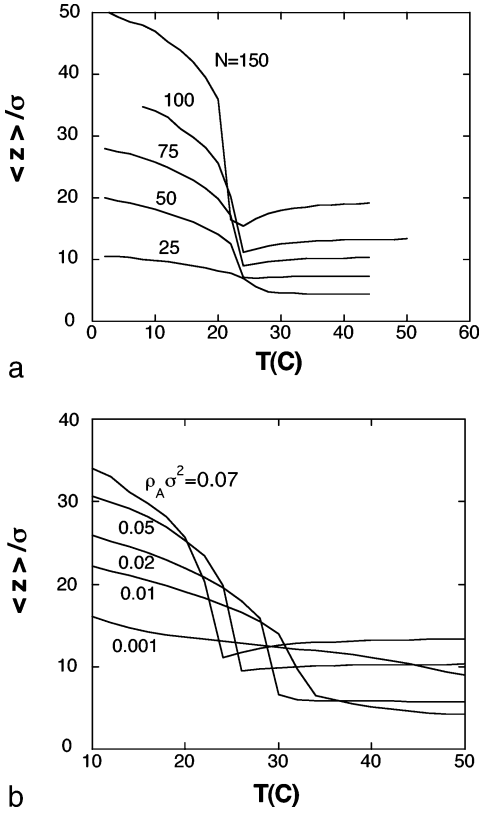

Figure 7. (a) First moment of the polymer volume fraction profile as a function of temperature where $\rho_A\sigma^2$ is held constant at 0.07 and N is varied as indicated on the plot. (b) First moment of the polymer volume fraction profiles as a function of temperature where N is held fixed at 100 and the surface coverage is varied as indicated on the plot.

The apparent transition calculated from our SCF theory depends on chain length and surface coverage. We observe from Figure 7a that the effect of increasing N is to sharpen the transition. We also observe that at lower $N(25)$ $\langle z \rangle$ varies smoothly and continuously over the entire temperature range and that the minimum immediately after the transition is no longer present. This supports our previous assertion about changes in the solvent quality being a function of the polymer concentration: the lower N films have lower volume fraction thus χ may not be at high enough ϕ to cause the solvent to become better with increasing temperature. Over the range of N we studied, increasing N is seen to shift the transition temperature to lower values by only a few degrees Celsius. It is known from experiments of free PNIPAM in solution that molecular weight has practically no effect on the demixing temperature[46,60,61] in contrast to polymer concentration which has an unambiguous effect as demonstrated in the phase diagrams reported by several authors.[46,62,63] SCF theory predicts that surface coverage indeed has a

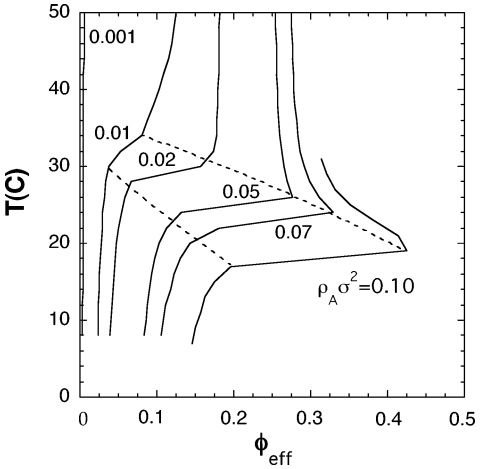

Figure 8. Temperature vs the effective monomer fraction ϕ_{eff} at fixed chain length $N = 100$ for a range of surface coverages $\rho_A\sigma^2$ indicated in the plot. The dashed line is a sketch of the apparent coexistence curve.

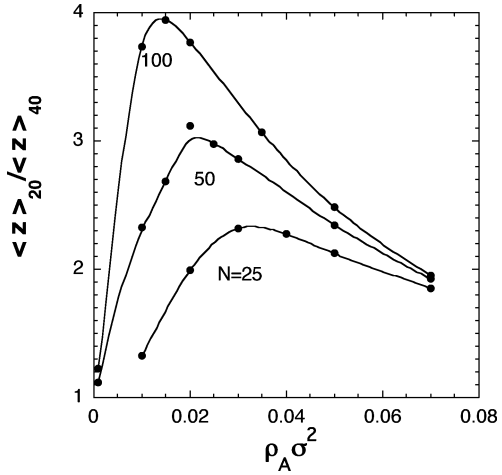

Figure 9. Ratio of first moments at 20 and 40 °C is plotted vs the surface coverage $\rho_A\sigma^2$ for various chain lengths N indicated.

significant effect on the transition temperature as shown in Figure 7b. Increasing $\rho_A\sigma^2$ from 0.001 to 0.07 with N held constant causes the transition temperatures to shift to much lower values.

It is instructive to plot the results from Figures 7 as a function of an effective monomer volume fraction ϕ_{eff} within the tethered layer

$$\phi_{eff} = \frac{\pi N \rho_A \sigma^3}{6\langle z \rangle} \tag{15}$$

Note that our definition of ϕ_{eff} is somewhat different than our earlier definition of $\langle\phi\rangle$ in eq 4 for the reference system. Only for a step function profile are ϕ_{eff} and $\langle\phi\rangle$ the same; in general they are not equal since $\langle\phi\rangle$ depends on the details of the profile. In Figure 8, we plotted temperature vs the effective volume fraction of monomer for a range of surface coverages. Starting at low temperature, if we follow a constant surface coverage curve, we find that ϕ_{eff} increases slightly with T as the layer thickness $\langle z\rangle$ initially decreases. Upon further temperature increase, we observe an abrupt increase in ϕ_{eff} consistent with a first-order transition. Finally, at sufficiently high surface coverage, we notice that ϕ_{eff} decreases with temperature as the tethered layer thickness increases as seen in Figure 7.

The dashed curves sketched in Figure 8 suggest a coexistence regime for the tethered chain system analogous to the bulk phase diagram in Figure 1 of the aqueous PNIPAM solution. With this interpretation, we see that the tethering constraint on the chains has the effect of distorting the coexistence region that free chains experience in bulk solution. Note that at the lowest surface coverage of $\rho_A\sigma^2 = 0.001$ no discontinuous change in ϕ_{eff} is observed. Thus, one would expect an upper critical solution temperature (UCST) to appear between surface coverages of 0.001 and 0.01, even though the experimental phase diagram shows only an LCST in the temperature range 20−40 °C. At very high surface coverages, we expect that the tethered chains would be forced into completely extended configurations at all temperatures due to steric constraints. Although it is not apparent from Figure 8, these considerations suggest that at very high ϕ_{eff}, the coexistence region of the tethered system would close off and exhibit an LCST. Thus, we speculate that the effective phase diagram of the tethered chain system would be of the closed loop type.

In applications of grafted PNIPAM surfaces, one is frequently interested in the relative change in the layer thickness when the temperature is switched between fixed low and high temperatures. To illustrate this, in Figure 9, we plotted our SCF predictions of the ratio of layer thicknesses at $T = 20$ and 40 °C as a function of the surface coverage. It can be seen that the relative magnitude of the effect is nonmonotonic and is maximized at an intermediate value of the surface coverage. Furthermore, the surface coverage corresponding to the maximum effect shifts to lower values as the chain length is increased.

IV. Conclusions

Tethered PNIPAM chains were studied with a self-consistent field theory derived from density functional theory under the approximation that the field is local. Information regarding the statistical mechanics of the bulk polymer solution of PNIPAM in water was directly inputted to the theory through the composition dependent χ parameter determined experimentally by Afroze et al.[46] Below the LCST of the bulk solution, the tethered PNIPAM chains were well solvated and the composition profile extended into the water. Conversely, above the LCST of the bulk solution, the tethered PNIPAM chains were localized near the surface in an attempt to minimize contact with solvent molecules.

An apparent first-order change in layer thickness was observed at a temperature depending on surface coverage and chain length. Unlike the previous mean field calculations of Baulin and Halperin[44] we found no evidence of *vertical phase separation* within the tethered layer. This is to be expected since in our SCF calculations the χ parameter does not vary with distance from the wall, but is essentially averaged over the layer thickness (see eq 4). On the basis of our results over a limited range of surface coverage and chain length, we find that the tethering constraint has the effect of distorting the phase diagram of the uniform PNIPAM solution. Moreover, we speculate that the phase coexistence regime of the tehthered PNIPAM/water system is closed, exhibiting both a UCST and LCST. As a consequence, the relative magnitude of the layer collapse at low and high temperature is nonmonotonic with a maximum effect occurring at a surface coverage that

decreases with increasing chain length in qualitative agreement with experiment.[9]

Acknowledgment. Sandia is a multiprogram laboratory operated by Sandia Corporation, a Lockheed Martin Company, for the United States Department of Energy's National Nuclear Security Administration under Contract No. DE-AC04-94AL85000. G.P.L. acknowledges funding from the Office of Naval Research N00014-02-1-0377. The authors would like to thank Michael Kent for helpful discussions and suggestions.

References and Notes

(1) Schild, H. G. *Prog. Polym. Sci.* **1992**, *17*, 163.
(2) Mendez, S.; Ista, L. K.; Lopez, G. P. *Langmuir* **2003**, *19*, 8115.
(3) Ista, L. K.; Mendez, S.; Perez-Luna, V. H.; Lopez, G. P. *Langmuir* **2001**, *17*, 2552.
(4) Huber, D. L.; Manginell, R. P.; Samara, M. A.; Kim, B. L.; Bunker, B. C. *Science* **2003**, *301*, 352.
(5) Fu, Q.; Rama Rao, G. V.; Ista, L. K.; Wu, Y.; Andrzejewski, B.; Sklar, L. A.; Ward, T. L.; Lopez, G. P. *Adv. Mater.* **2003**, *15*, 1262.
(6) Kent, M. S. *Macromol. Rapid Commun.* **2000**, *21*, 243.
(7) Karim, A.; Satija, S. K.; Douglas, J. F.; Ankner, J. F.; Fetters, L. J. *Phys. Rev. Lett.* **1994**, *73*, 3407.
(8) Yim, H.; Kent, M. S.; Huber, D. L.; Satija, S.; Majewski, J.; Smith, G. S. *Macromolecules* **2003**, *36*, 5244.
(9) Yim, H.; Kent, M. S.; Mendez, S.; Balamurugan, S. S.; Balamurugan, S.; Lopez, G. P.; Satija, S. *Macromolecules* **2004**, *37*, 1994.
(10) Balamurugan, S.; Mendez, S.; Balamurugan, S. S.; O'Brien, M. J., II; Lopez, G. P. *Langmuir* **2003**, *19*, 2545.
(11) Kidoaki, S.; Ohya, S.; Nakayama, Y.; Matsuda, T. *Langmuir* **2001**, *17*, 2402.
(12) Jones, D. M.; Smith, J. R.; Huck, W. T. S.; Alexander, C. *Adv. Mater.* **2002**, *14*, 1130.
(13) Szleifer, I.; Carignano, M. A. *Adv. Chem. Phys.* **1996**, *44*, 165.
(14) Halperin, A.; Tirrell, M.; Lodge, T. P. *Adv. Polym. Sci.* **1992**, *100*, 31.
(15) Milner, S. T. *Science* **1991**, *251*, 905.
(16) Alexander, S. J. *J. Phys. (Paris)* **1977**, *38*, 983.
(17) de Gennes, P. G. *Macromolecules* **1980**, *13*, 1069.
(18) de Gennes, P. G. *C. R. Acad. Sci. Paris* **1985**, *300*, 839.
(19) Scheutjens, J. M. H. M.; Fleers, G. J. *J. Phys. Chem.* **1979**, *83*, 1619.
(20) Cosgrove, T.; Heath, T.; van Lent, B.; Scheutjens, J. M. H. M. *Macromolecules* **1987**, *20*, 1692.
(21) Shull, K. R. *J. Chem. Phys.* **1991**, *94*, 5723.
(22) Baranowski, R.; Whitmore, M. D. *J. Chem. Phys.* **1998**, *108*, 9885.
(23) Martin, J. I.; Wang, Z. G. *J. Phys. Chem.* **1995**, *99*, 2833.
(24) Laradji, M.; Guo, H.; Zuckermann, M. J. *Phys. Rev. E* **1994**, *49*, 3199.
(25) Muthukumar, M.; Ho, J. S. *Macromolecules* **1989**, *20*, 965.
(26) Milner, S. T.; Witten, T. A.; Cates, M. E. *Macromolecules* **1988**, *21*, 2610.
(27) Milner, S. T. *J. Chem. Soc., Faraday Trans.* **1990**, *86*, 1349.
(28) Milner, S. T. *Eur. Phys. J.* **1988**, *7*, 695.
(29) Cosgrove, T. *J. Chem. Soc., Faraday Trans.* **1990**, *86*, 1323.
(30) Zhulina, E. B.; Borisov, O. V.; Pryamitsyn, V. A.; Birshtein, T. M. *Macromolecules* **1991**, *24*, 140.
(31) Pincus, P. *Macromolecules* **1991**, *24*, 2912.
(32) Halperin, A. *Eur. Phys. J. B* **1998**, *3*, 359.
(33) Grest, G. S.; Murat, M. *J. Chem. Phys.* **1996**, *105*, 5532.
(34) Murat, M.; Grest, G. S. *Macromolecules* **1989**, *22*, 4054.
(35) Murat, M.; Grest, G. S. *Macromolecules* **1991**, *24*, 704.
(36) Grest, G. S.; Murat, M. *Macromolecules* **1993**, *26*, 3108.
(37) Grest, G. S. *Macromolecules* **1994**, *27*, 418.
(38) Lai, P. Y.; Binder, K. *J. Chem. Phys.* **1992**, *97*, 586.
(39) Baranowski, R.; Whitmore, M. D. *J. Chem. Phys.* **1995**, *103*, 2343.
(40) Kent, M. S.; Lee, L. T.; Factor, B. J.; Rondelez, F.; Smith, G. S. *J. Chem. Phys.* **1995**, *103*, 2320.
(41) Kent, M. S.; Majewski, J.; Smith, G. S.; Lee, L. T.; Satija, S. *J. Chem. Phys.* **1998**, *108*, 5635.
(42) Bjorling, M.; Linse, P.; Karlstrom, G. *J. Phys. Chem.* **1990**, *94*, 471.
(43) Karlstrom, G. *J. Phys. Chem.* **1985**, *89*, 4962.
(44) Baulin, V. A.; Halperin, A. *Macromol. Theor. Simul.* **2003**, *12*, 549.
(45) Baulin, V. A.; Zhulina, E. B.; Halperin, A. *J. Chem. Phys.* **2003**, *119*, 10977.
(46) Afroze, F.; Nies, E.; Berghmans, H. *J. Mol. Struct.* **2000**, *554*, 55.
(47) McCoy, J. D.; Ye, Y.; Curro, J. G. *J. Chem. Phys.* **2002**, *117*, 2975.
(48) Carignano, M. A.; Szleifer, I. *J. Chem. Phys.* **1993**, *98*, 5006.
(49) Ye, Y.; McCoy, J. D.; Curro, J. G. *J. Chem. Phys.* **2003**, *119*, 555.
(50) Chandler, D.; McCoy, J. D.; Singer, S. J. *J. Chem. Phys.* **1986**, *85*, 5971.
(51) McCoy, J. D.; Teixeira, M. A.; Curro, J. G. *J. Chem, Phys.* **2001**, 114, 4289.
(52) Nath, S. K.; McCoy, J. D.; Curro, J. G.; Saunders, R. S. *J. Polym. Sci., B: Polym. Phys.* **1995**, *33*, 2307. Nath, S. K.; McCoy, J. D.; Curro, J. G.; Saunders, R. S. *J. Chem. Phys.* **1997**, *106*, 1950. Nath, S. K.; McCoy, J. D.; Curro, J. G.; Saunders, R. S. *J. Chem. Phys.* **1998**, *108*, 3023.
(53) Hooper, J. B.; McCoy, J. D.; Curro, J. G. *J. Chem. Phys.* **2000**, *112*, 3090. Hooper, J. B.; Pileggi, M. T.; McCoy, J. D.; Curro, J. G.; Weinhold, J. D. *J. Chem. Phys.* **2000**, *112*, 3094. Hooper, J. B.; McCoy, J. D.; Curro, J. G.; van Swol, F. *J. Chem. Phys.* **2000**, *113*, 2021.
(54) Hansen, J. P.; McDonald, I. R. *Theory of Simple Liquids*; Academic Press: London, 1986.
(55) Schweizer, K. S.; Curro, J. G. *Adv. Chem. Phys.* **1997**, *98*, 1.
(56) Flory, P. J. *Principles of Polymer Chemistry*; Cornell University Press: Ithaca, NY, 1953.
(57) Kirkwood, J. G.; Buff, F. P. *J. Chem. Phys.* **1951**, *19*, 774.
(58) Israelachvili, J. N. *Intermolecular and Surfaces Forces*, 2nd ed.; Academic Press: New York, 1992.
(59) Yim, H.; Kent, M. S.; Satija, S.; Mendez, S.; Balamurugan, S. S.; Balamurugan, S.; Lopez, G. P. *J. Polym. Sci., Part B: Polym. Phys.* **2004**, *42*, 3302.
(60) Fujishige, S.; Kubota, K.; Ando, I. *J. Phys. Chem.* **1989**, *93*, 3311.
(61) Schild, H. G.; Tirell, D. A. *J. Phys. Chem.* **1990**, *94*, 4352.
(62) Marchetti, M.; Prager, S.; Cussler, E. L. *Macromolecules* **1990**, *23*, 1760.
(63) Heskins, M.; Guillet, J. E. *J. Macromol. Sci. Chem.* **1968**, *A2*, 1441.

MA048156X